JMEPEG (2012) 21:739–747
DOI: 10.1007/s11665-012-0182-7

1059-9495/$19.00

Fatigue Assessment of Defect-Free and Defect-Containing Brazed Steel Joints

Christian Leinenbach, Michael Koster, and Hans-Jakob Schindler

(Submitted October 20, 2011; in revised form January 16, 2012)

This work aims at the development of lifetime estimation procedures for defect-free and defect-containing brazed joints. Preliminary investigations were performed to measure the influence of specimen geometry on the joint strength. To estimate the influence of defects on the fatigue lifetime, defect-free specimens were compared with specimens containing defects. The experiments show that defect-containing specimens provide considerably lower joint strengths than defect-free specimens. The decrease of the fatigue strength with increasing defect size can be shown, but the direct comparison of different defects is not possible with S-N-curves. Based on the experimental results and on theoretical investigations, a procedure was developed to estimate the lifetime of defect-free and defect-containing brazed joints based on the stress intensity caused by a defect.

Keywords brazing, brazing defects, defect assessment, fatigue behavior, lifetime estimation

1. Introduction

Brazing is a method of consistent joining for a wide range of materials. Besides the reliability, fast processing time and the low manufacturing costs, especially the comparably low process temperatures qualify brazing for many industrial applications, e.g., for the production of power electronic components, but also in automotive engineering and for power generation. Simultaneously, brazing provides potentials for seminal applications, e.g., for the production of structures for particle accelerators (Ref 1), in aerospace technology (Ref 2), as well as for heat exchanging systems for hydrogen energy production (Ref 3). Especially, brazing of steel structures becomes more economical and efficient with the use of advanced furnace brazing methods (Ref 4), as, e.g., high temperature (HT) furnace brazing in vacuum or with a shielding gas. HT furnace brazing is performed at temperatures $>900°$ C for the production of highly loaded components, such as turbo compressor impellers or turbine parts (Ref 5). Many of the above-mentioned components are exposed to complex loading conditions in service, comprising mechanical, thermal, or thermo-mechanical loads.

Brazings form heterogeneous, anisotropic systems, consisting of the base material, the filler metal, and the diffusion zone. Under mechanical loading, the properties of the system vary significantly from those of the individual joining partners. The different elastic-plastic properties of the filler metal and the base material lead to a triaxial stress state in the brazing zone, caused by constraining effects of the base material on the filler alloy. As a result, large hydrostatic stresses occur in the braze layer and the ultimate tensile strength of the joint can be several times higher than the strength of the unconstrained layer material (Ref 6, 7). The mechanical performance of such constrained systems under static loading has been studied extensively in the past (e.g. Ref 8-12).

Considering the integrity of a brazed component, especially the influence of (brazing) defects is of significant importance. Typical defects that can occur during brazing are incomplete gap filling due to local contaminations and poor wetting, pores due to entrapped gas or air or cracks as a result of residual stresses due to different thermal expansion coefficients of the joining partners and/or the presence of hard and brittle phases in the brazing zone (Ref 13). To estimate the influence of defects on bulk materials and on welded structures, defect assessment procedures, such as R6, BS7910, or SINTAP, based on the so-called failure assessment diagrams (FAD) have been developed for static loading conditions (Ref 14-17). In our previous investigations, it could be shown that the FAD concept can be also used to estimate the influence of defects that occur during brazing (Ref 18, 19).

To provide structural reliability for brazed components in service, their behavior under cyclic loading needs to be considered, too. The fatigue behavior of brazed components is much more complex in comparison with bulk materials and has hardly been considered in the literature yet (Ref 20, 21). A number of studies on the fatigue crack propagation behavior at or near interfaces in constrained layers (e.g., in adhesively bonded joints, metal-ceramic joints, or multi-layered materials) have been published in the past two decades (e.g., Ref 22-24).

This article is an invited submission to JMEP selected from presentations at the Symposia "Wetting, soldering and brazing" and "Diffusion bonding and characterization" belonging to the Topic "Joining" at the European Congress and Exhibition on Advanced Materials and Processes (EUROMAT 2011), held September 12-15, 2011, in Montpellier, France, and has been expanded from the original presentation.

Christian Leinenbach and **Michael Koster**, Laboratory of Joining and Interface Technology, EMPA-Swiss Federal Laboratories for Materials Science and Technology, Ueberlandstrasse 129, 8600 Dübendorf, Switzerland; and **Hans-Jakob Schindler**, Mat-Tec AG, Winterthur, Switzerland. Contact e-mail: christian.leinenbach@empa.ch.

Nomenclature

Roman Symbols

a, mm	Crack/defect length
a_n, mm	Depth of initial notch
$A_{fatigue}$, mm^2	Fatigue fracture surface
A_{res}, mm^2	Residual fracture surface
d, mm	Thickness of the braze layer
K_{fc}, MPa $m^{1/2}$	Critical stress intensity factor in fatigue
K_{IN}, MPa $m^{1/2}$	Stress intensity in a sharp notch
K_{Ic}, MPa $m^{1/2}$	Fracture toughness
$K_{I,max}$, MPa $m^{1/2}$	Maximum stress intensity
$K_{th,max}$, MPa $m^{1/2}$	Stress intensity threshold
ΔK_I, MPa $m^{1/2}$	Stress intensity range
n_{Paris}, -	Paris exponent
N_{ini}, -	Number of loading cycles for crack formation
N_f, -	Number of cycles to fracture
N_{tot}, -	Total fatigue lifetime
N_{max}, -	Maximum number of cycles (2×10^4 for the following investigations)
N_{prop}, -	Number of loading cycles for crack propagation
N_{is}, -	Number of loadings at the LCF/HCF-SIF intersection
R, -	Load ratio
S_{IF}, MPa $m^{1/2}$	Stress intensity factor
T, mm	Specimen length
W, mm	Specimen width
Y_{se}, -	Dimensionless factor for the calculation of $K_{I,max}$

Greek Symbols

ρ, mm	Notch root radius
σ_f, MPa	Ultimate tensile strength
σ_y, MPa	Yield strength
$\Delta\sigma_{nom}$, MPa	Applied nominal stress range
$\Delta\sigma_{nom,20000}$, MPa	Maximum tolerable nominal stress range until N_{max}
σ_{notch}, MPa	Maximum local stress in a notch

In their previous works, the present authors investigated the fatigue crack propagation in braze joints. It was shown that the joints are characterized by the absence of a clear short crack regime, a relatively high threshold value ΔK_{th} as well as by an unusually high Paris exponent (Ref 25-27). While for most metals, the Paris exponent n_{Paris} is known to be between 3 and 4 in the stable crack-growth regime (Ref 28), it was estimated between 11 and 13 for brazed martensitic stainless steel components. In addition, a concept for the consideration of residual stresses in the braze layer on the fatigue crack behavior of brazed components was developed (Ref 29). However, these studies do not cover the crack initiation stage and therefore cannot be used for making predictions of the whole fatigue lifetime of brazed components.

Considering the influence of pores or partly unfilled brazing gaps—which can be considered as sharp notches in the brazing zone rather than cracks—on the fatigue behavior of brazed joints no information is available in the literature.

In the current work, the fatigue behavior of brazed steel joints under axial loading was studied. By the combination of experimental testing methods and theoretical models, a method for estimating the fatigue life of defect-free and defect-containing brazed joints based on stress concentration factors was developed.

2. Experimental Investigations

2.1 Materials, Brazing Process, and Specimen Preparation

For the following investigations, the soft martensitic stainless steel X3CrNiMo13-4 (AISI CA 6-NM) was used as base material for the brazings. It is characterized by a martensitic-ferritic microstructure, providing high strength after heat treatment (Fig. 1a). Due to its excellent mechanical properties and corrosion behavior as well as its thermal resistance, the steel is widely used for pumps, compressors, or water turbines. Brazing was performed using foils of the binary alloy Au-18Ni

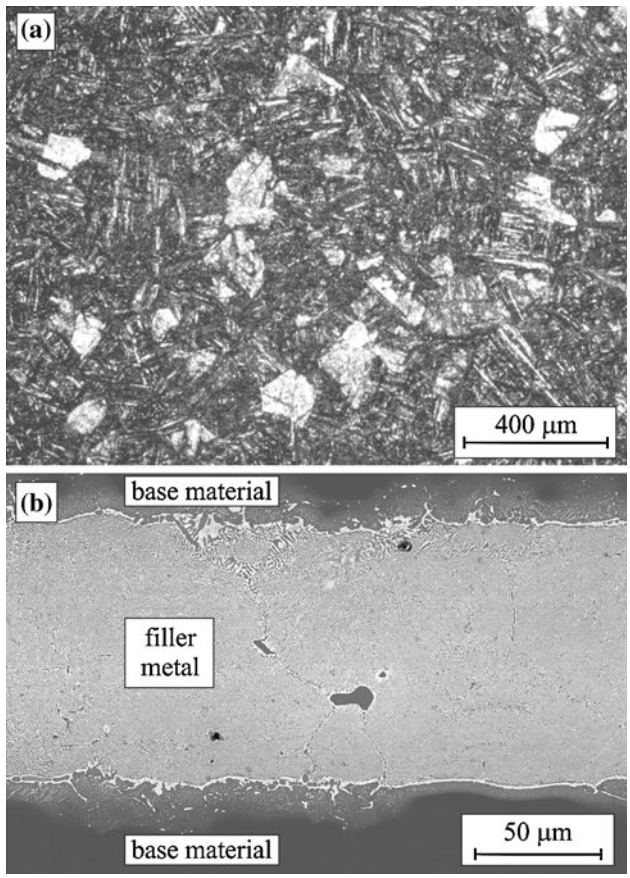

Fig. 1 Microstructure of (a) the base material and (b) the brazed joint

($T_m \approx 955$ °C) with a thickness of 100 µm as filler metal. Steel plates with the dimensions $300 \times 100 \times 25$ mm were brazed using a special brazing jig. The brazing process was performed

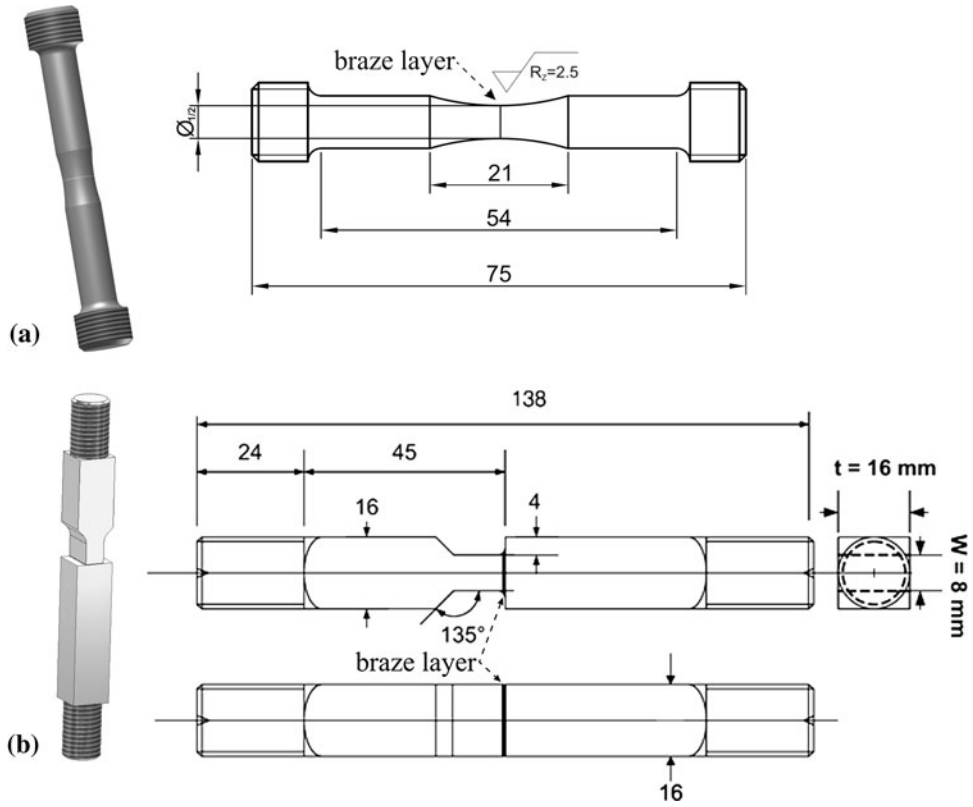

Fig. 2 The geometry of (a) the standard round specimens and (b) the T-joint specimen

in an industrial shielding gas furnace (SOLO Profitherm 600) at a temperature of 1020 °C for 20 min. After brazing, the specimens were tempered at 520 °C for 5.5 h in nitrogen atmosphere. Figure 1(b) shows the microstructure of the braze joint.

Besides standard round tensile specimens, round fatigue specimens with gauge length diameters of $Ø_1 = 4$ mm and $Ø_2 = 5$ mm were used for the experiments (Fig. 2a). Furthermore, special T-joint geometry specimens (Fig. 2b) were manufactured to determine the geometry effect on the joint strength. This geometry is often realized in technical components. The T-joint specimens are characterized by an abrupt change of the cross section and consequently by the highest loads, occurring in the braze layer. This geometry was also used to study the influence of brazing defects on the mechanical properties. Therefore, defects of different geometries (straight and semi-elliptical) and sizes were introduced into the brazing zone by electrical discharge machining (EDM), using a wire with a diameter of 0.3 mm (Fig. 3).

To investigate the influence of the defect size, specimens containing straight defects with a size of $a = 0.5$ mm, $a = 1$ mm, and $a = 2$ mm were prepared. For the semi-elliptical defects, a ratio of $a/c = 2/3$ with $a = 0.75$ mm, $a = 1.5$ mm, and $a = 3$ mm was selected. With this, typical brazing defects like a partly unfilled brazing gap or large pores should be simulated. With respect to their three-dimensional geometry, the defects can be considered as sharp notches.

2.2 Testing Procedures

In order to determine the quasistatic mechanical properties of the braze joints, tensile tests were performed with an electromechanical testing machine (Schenck Trebel RSA 250 kN).

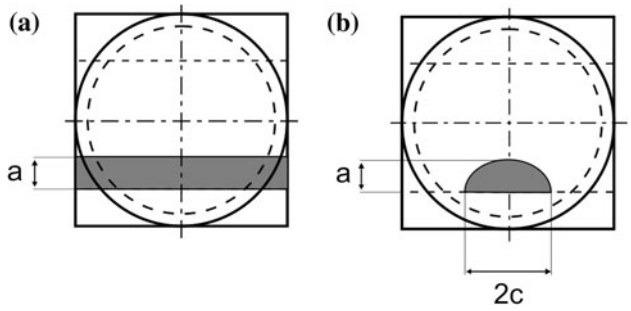

Fig. 3 Defect geometries of (a) straight and (b) semi-elliptical defects

For the simulation of start/stop cycles of highly loaded brazed components, the fatigue behavior in the LCF regime was characterized with a servohydraulic testing machine (Schenk Hydroplus 5666) until a maximum number of loading cycles of $N_{max} = 2 \times 10^4$ cycles. The tests were performed with a sinusoidal load, applied with a constant amplitude at a frequency of 1 Hz and at a load ratio of $R = 0.1$.

2.3 Behavior of Joints Under Quasistatic Loading

To characterize the influence of different specimen geometries and of different defects on the quasistatic joint strength, tensile tests were performed. Therefore, standard round specimens according to DIN 50125 were tested. Their values served as a reference for the further experiments. The average ultimate tensile strength (σ_f) of standard round specimens is 1084 MPa. Experiments with T-joint specimens show that the change of the specimen geometry leads to a slight increase of σ_f to

Table 1 Comparison of joint strength of defect-free specimens with different geometries and estimated fatigue strengths to an ultimate number of cycles of $N_f = 2 \times 10^4$

Specimen geometry	σ_f, MPa	$\Delta\sigma_{nom,20000}$, MPa
Base material	1224 ± 2	…
T-Joint specimen	1120 ± 4.8	405
Standard round	1084 ± 3.6	720

Table 2 Comparison of joint strength of specimens and estimated fatigue strengths to an ultimate number of cycles of $N_f = 2 \times 10^4$ from the S-N-curves for different defect geometries and sizes

Defect type	Defect size, a, mm	σ_f, MPa	$\Delta\sigma_{nom,20000}$, MPa
Defect free	0	1120	405
Straight	0.5	…	270
	1	570	180
	2	447	135
Semi-elliptical	0.75	…	360
	1.5	927	282
	3	699	270

1120 MPa. The results of the tensile tests are summarized in Table 1.

Further tensile tests were performed to study the influence of the different defects on the joint strength. For all experiments, the ultimate tensile strength and the maximum tolerable stress range for the specimens to reach N_{max} without failure ($\Delta\sigma_{nom,20000}$) were calculated. As expected, defect-containing specimens showed considerably lower tensile strengths, compared to the defect-free reference specimens. The decrease of the tensile strength is closely related to the size and the shape of the introduced defect. The lowest ultimate tensile strength of $\sigma_f = 453$ MPa was obtained for a specimen containing a straight defect with a depth of 2 mm. The results are in good agreement with the results reported in (Ref 6) and are summarized in Table 2.

2.4 Behavior of Joints Under Cyclic Loading

Fatigue tests were performed to investigate the influence of the specimen geometry and of defects on the LCF fatigue behavior. Round-shaped specimens, which serve as a reference, as well as T-joint specimens, were used (Fig. 4).

The results of the fatigue experiments with defect-free specimens until $N_{max} = 2 \times 10^4$ cycles show a significant effect of the specimen geometry on the course of the measured S-N-curves. For standard round-shaped specimens, the fatigue strength to 20,000 cycles, $\Delta\sigma_{nom,20000}$, can be estimated to 720 MPa, whereas the fatigue strength for defect-free T-joint specimens was 405 MPa. Figure 5 shows the resulting S-N-curves for specimens containing straight defects, and semi-elliptical defects with different sizes. The results from the defect-free T-joint specimens were considered as a reference in the two diagrams.

As expected, the investigations show that defect-containing specimens provide significantly lower $\Delta\sigma_{nom,20000}$, compared to the defect-free reference specimens. The reduction of $\Delta\sigma_{nom,20000}$ is influenced not only by the size of the defect

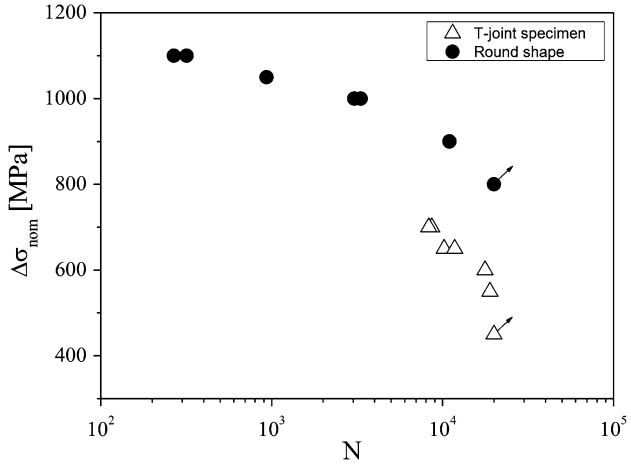

Fig. 4 Comparison of the S-N-curves of defect free T-joint specimens and of round specimens

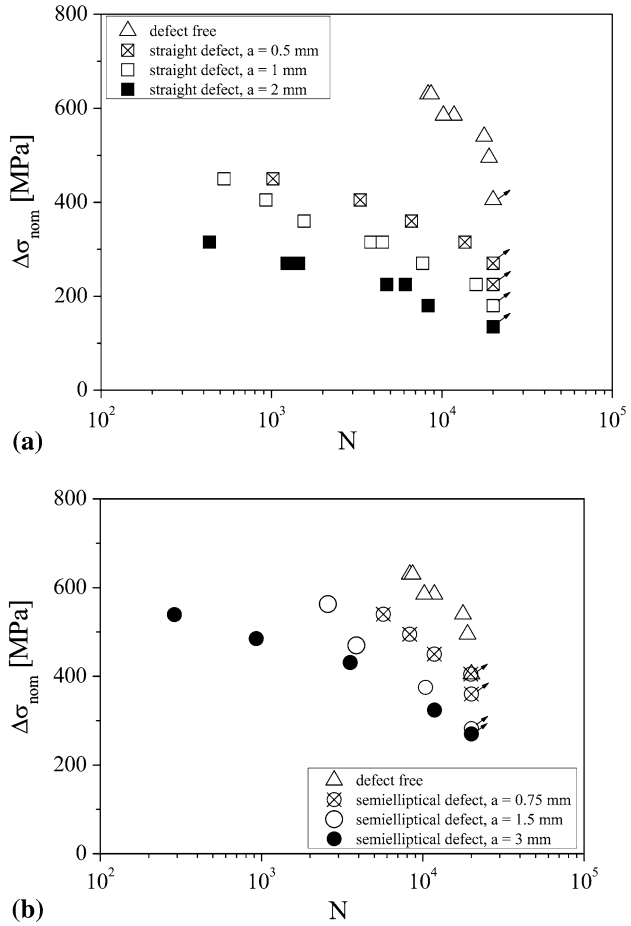

Fig. 5 S-N-curves for specimens containing (a) straight and (b) semi-elliptical defects

but also by its shape. Considering the defect geometry, the decrease of $\Delta\sigma_{nom,20000}$ is more pronounced for straight defects compared to semi-elliptical defects. For example, a straight defect with a size of $a = 2$ mm led to a reduction of $\Delta\sigma_{nom,20000}$ to 135 MPa, whereas a joint with a semi-elliptical defect with $a = 3$ mm survived $\Delta\sigma_{nom,20000} = 270$ MPa damage-free. Furthermore, although $\Delta\sigma_{nom,20000}$ of the specimen

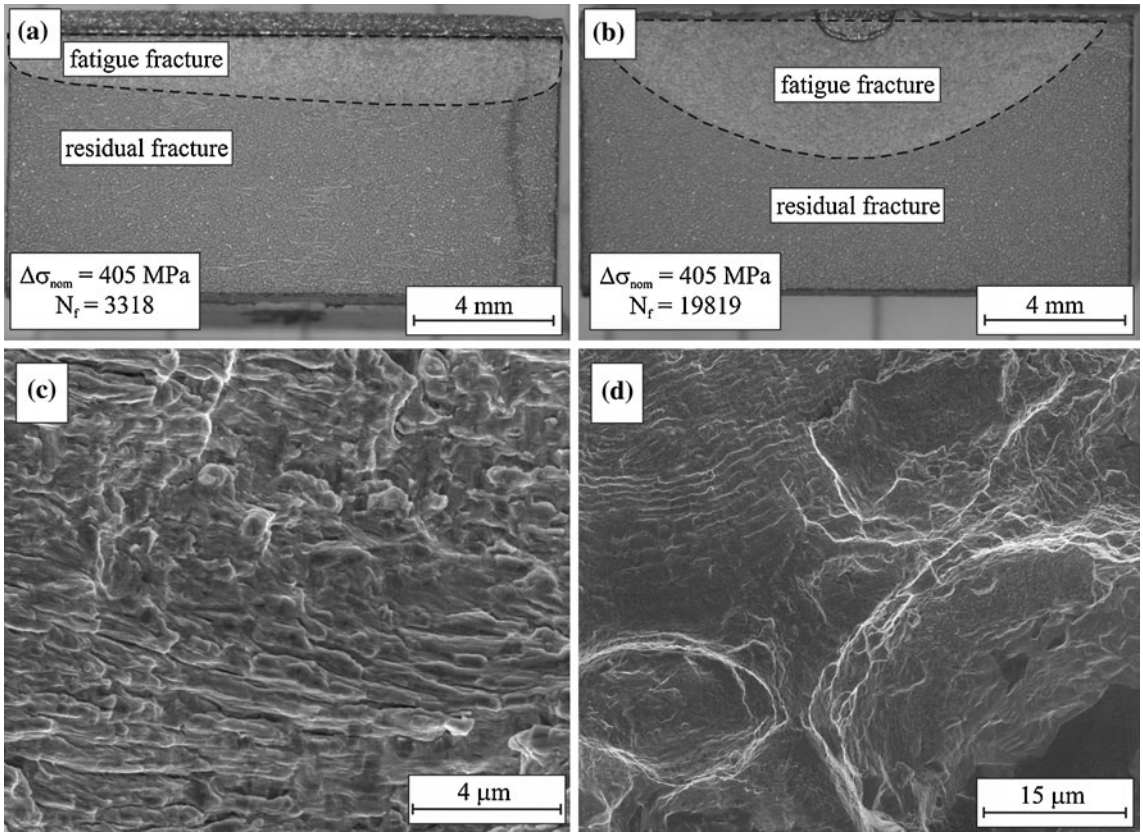

Fig. 6 Fractographic investigations of a T-joint specimen, containing (a) a straight and (b) a semi-elliptical defect, (c) of the fatigue fracture surface, and (d) at the transition between fatigue and residual fracture surface

with the smallest straight defect (a = 0.5 mm in Fig. 5) is expected to be the closest to the defect-free specimens, the smallest semi-elliptical defect (a = 0.75 mm in Fig. 5) exhibited the highest tolerable stress range of $\Delta\sigma_{nom,20000}$ = 360 MPa, and almost reaches $\Delta\sigma_{nom,20000}$ of the defect-free reference specimen (Table 2).

2.5 Fractographic Investigations

After the fatigue tests, the fracture surfaces of the T-joints were characterized by stereo microscopy. All specimens clearly fractured in the brazing zone as residual filler alloy was detected on both parts of the fractured specimens.

Figure 6(a) shows a specimen containing a straight defect with a size of 0.5 mm, that failed after N_f = 3,318 loading cycles $\Delta\sigma_{nom}$ = 405 MPa. A specimen containing a semi-elliptical defect with a = 0.75 mm, exhibited 19,819 loading cycles at the same loading amplitude (Fig. 6b). The fracture surfaces can be clearly divided into a fatigue fracture surface ($A_{fatigue}$) and residual fracture surface (A_{res}). An increase in the number of cycles to fracture leads to an increase in $A_{fatigue}$. While $A_{fatigue}$ amounts 24.18% for the specimen shown in Fig. 6(a), it increases to 32.49% for higher N_f (Fig. 6b). For the specimens containing semi-elliptical defects, the a/c ratio changed slightly from 0.67 to approximately 0.55 to 0.6 until final fracture as determined from the fatigue fracture areas.

SEM investigations have shown that $A_{fatigue}$ is characterized by a smooth fracture surface and contains fatigue-induced deformation features, as, e.g., striations (Fig. 6c). SEM investigations at the transition from fatigue to residual fracture surface show a pronounced increase of the striation spacing from $<$100 to $\approx$1000 nm, what is in good agreement with the measured crack growth curves (Ref 26). The residual fracture surface is characterized by ductile deformation features like dimples (Fig. 6d).

2.6 Correlation of Fatigue Life with ΔK

In cases of joints with large brazing defects the nominal stress is not a suitable parameter to correlate the fatigue life, as can be seen from the test data (Fig. 5). Therefore, a lifetime prediction or a safety analysis for a component containing brazing defects cannot be done in a reasonable way based on S-N-curves.

As shown in Ref 24, the loading state of a crack-like defect in a thin layer can be characterized by the global stress intensity factor (SIF) of a crack with the same geometry and size in a corresponding homogeneous body. In Fig. 7, the data shown in Fig. 5 are plotted as a function of $\Delta K(a_n)$, the latter being the range of the SIF of a hypothetical crack of the same length as the defect, $a = a_n$, under mode I loading. The SIFs for the defects in the tests specimens are calculated as follows:

For a straight crack of length a emanating from the corner of a T-Joint, the SIF is given by (Ref 29)

$$K_I = 2.293 \cdot \sigma_{nom} \cdot \sqrt{W} \cdot \sqrt{\frac{a}{W} + 0.0338} \cdot Y_{st}(a/W) \qquad \text{(Eq 1)}$$

For $a/W > 0.01$, the non-dimensional function $Y_{st}(a/W)$ is given by

$$Y_{st}(a/W) = 1 - 0.5454 \cdot \left(\frac{a}{W}\right) + 5.8863 \cdot \left(\frac{a}{W}\right)^2 - 8.9417 \cdot \left(\frac{a}{W}\right)^3 + 15.809 \cdot \left(\frac{a}{W}\right)^4. \quad \text{(Eq 2)}$$

Note that Eq 1 and 2 can also be used as a conservative estimation of the SIF for short cracks in the range $a/W < 0.01$, as discussed in section 3.2.

For the semi-elliptical defects with $a/c = 2/3$ emanating from the corner of a T-Joint, the SIF as derived in Ref 18 can be approximated by the following formula:

$$K_I = 2.293 \cdot \sigma_{nom} \cdot \sqrt{W} \cdot Y_{se}\ (a/W) \quad \text{(Eq 3)}$$

with

$$Y_{se}(a/W) = \left(\frac{a}{W}\right)^{0.196} \cdot \left[0.9644 - 0.5641 \cdot \left(\frac{a}{W}\right)\right]. \quad \text{(Eq 4)}$$

With $a = a_n$, the test data from Fig. 5 can be represented as a function of $\Delta K(a_n)$ using Eq 1-4. The results are shown as SIF-N-curves in Fig. 7. Obviously they collapse in a relatively narrow scatter band, called in the following the SIF-N-curve. The correlation between $\log(N_{tot})$ and $\Delta K_I(a_n)$ is approximately linear and follows the regression line

$$\Delta K\ (a_n) = 70.533 - 11.781 \cdot \log N_{tot}. \quad \text{(Eq 5)}$$

The good correlation between N_{tot} is somewhat surprising since the total life of a notched specimen is expected to depend on many more parameters than just $\Delta K(a_n)$. However, there are theoretical reasons for $\Delta K(a_n)$ to be the main influencing factor of N_{tot}, as shown in section 3.1.

3. Theoretical Considerations

3.1 Relation Between Fatigue Life and ΔK

As mentioned above, the total fatigue life of a notched component, N_{tot}, can be divided into the number of load cycles required to form a crack at the notch tip, N_{ini}, and those required for crack propagation up to the critical crack length, N_{prop}, i.e.,

$$N_{tot} = N_{ini} + N_{prop}. \quad \text{(Eq 6)}$$

The transition from crack initiation to propagation cannot be clearly defined and is difficult to be detected experimentally. However, for the purpose of the present investigation, there is no need for a sharp distinction between these two phases of fatigue damage. N_{prop} can be obtained analytically quite uniquely. The fatigue crack propagation behavior of these brazings has been studied in Ref 24-26. It was found that the da/dN- versus ΔK-curves for brazed specimens do not exhibit the usual sigmoidal shape, but a Paris-type behavior in the entire range of crack growth. Correspondingly, the da/dN-curve can be approximated by

$$\frac{da}{dN} = C \cdot \Delta K^{n_{Paris}} \quad \text{(Eq 7)}$$

the entire range of ΔK, i.e., from the threshold value $K_{th,}$ to the critical SIF in fatigue, ΔK_{fc}. For $R = 0.1$, the parameters in Eq 7 were determined to be

$$C = 1.309 \times 10^{22} \quad \text{and} \quad n_{Paris} = 11.17. \quad \text{(Eq 8)}$$

ΔK_{fc} is obtained by

$$\Delta K_{fc} = \frac{K_{fc}}{1 - R} \quad \text{(Eq 9)}$$

where K_{fc} is fracture toughness in fatigue and a_c is the critical crack length, which is determined by the equation

$$\Delta K(a = a_c) = \Delta K_{cf}. \quad \text{(Eq 10)}$$

From Eq 7-10, the propagation life is obtained to be

$$N_{prop} = \int_{a_n}^{a_c} \frac{da}{C \cdot \Delta K_{n_{Paris}}(a)}. \quad \text{(Eq 11)}$$

Considering straight defects, Eq 7-10 inserted in Eq 11 result in the crack propagation life shown in Fig. 8. One can see that the propagation life as a function of $\Delta K(a_n)$ is nearly the same for all the considered defect sizes. The reason for this surprising behavior is the high value of the exponent n_{Paris}, which leads to an enormous acceleration of the crack growth rate as a approaches the critical length a_c. Therefore, $\Delta K(a_n)$

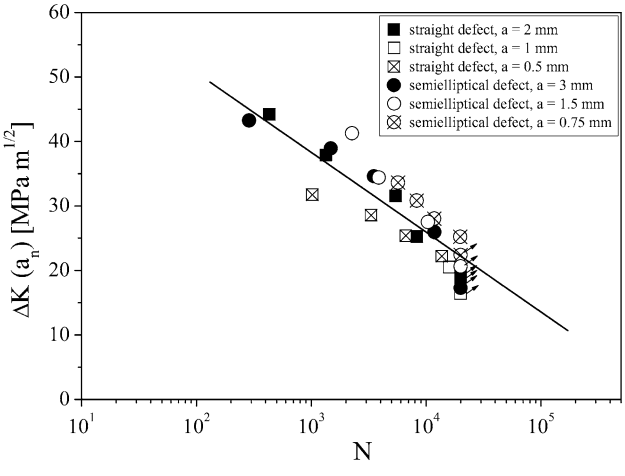

Fig. 7 SIF-N-curves for the estimation of the fatigue life of defect containing T-joint specimens

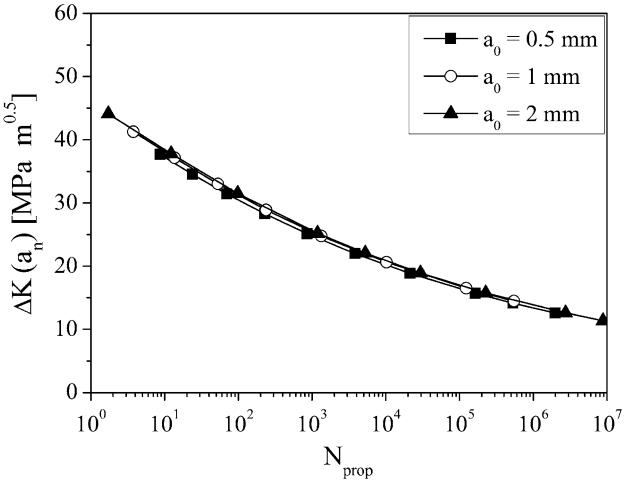

Fig. 8 Calculated crack-propagation life as a function of $\Delta K(a_n)$

has more significant influence on N_{prop} than $\Delta K(a_c)$. The same holds for other crack geometries such as the semi-elliptical cracks. So the above finding that N_{prop} depends on $\Delta K(a_n)$ only is likely to hold not only for the straight cracks considered in Fig. 8 but also for any crack shape.

In LCF, N_{ini} is known to be governed by the local plastic strain range $\Delta\varepsilon_p$. A dimensional analysis suggests a functional dependence of the form

$$\Delta\varepsilon_p = f\left(\frac{\Delta K^2(a_n)}{E \cdot \sigma_y \cdot d}\right) \quad \text{(Eq 12)}$$

where E is Young's modulus of the base material, σ_y the yield stress of the layer, and d the thickness of the layer. Thus,

$$N_{ini} = f(\Delta K(a_n), d). \quad \text{(Eq 13)}$$

Since N_{ini} as well as N_{prop} are functions of $\Delta K(a_n)$, it follows from Eq 6 that the total life of a notched brazing is mainly a function of $\Delta K(a_n)$, too. This is the theoretical reasons for the correlation shown in Fig. 7.

3.2 LCF at Structural Hot-Spots in Brazed Components

Even without a crack or defect, the T-shape of the specimen shown in Fig. 2(b) causes a stress-concentration similar to a notch. In the case of a brazing, the local notch radius, which in homogeneous materials is crucial for the magnitude of the stress concentration, is very difficult to define. Therefore, it is suitable and conservative to assume that a crack-like defect of a short initial length is present anyway. The SIF of a crack emanating from a sharp notch is characterized by a steep rise in the short crack range (I in Fig. 9) and a much flatter behavior in the long crack range (II in Fig. 9), with a relatively narrow transition range in between. Equations 1 and 2 only cover range II. Based on similar considerations for homogeneous materials (Ref 30), it is suggested in Ref 29 to characterize the stress state of a nominally defect-free T-joint with undefined local geometry by a notch-intensity factor K_{IN}, which is defined as an extrapolation of $K_I(a)$ in range II to $a = 0$ (Fig. 9). Physically, K_{IN} represents the maximum K_I that can occur at a short crack-like defect near a hot-spot. Mathematically, it is obtained from Eq 1 and 2 by setting $a = 0$, which results in

$$K_{IN} = K_I(a = 0) = 0.422 \cdot \sigma_{nom} \cdot \sqrt{W}. \quad \text{(Eq 14)}$$

By means of Eq 14, the fatigue life obtained by the tests on defect-free T-shaped specimens (Fig. 4) can be included in the SIF-N-correlation. The comparison is shown in Fig. 10, from which one can see that the corresponding ΔK_{IN}-N data are located well within in the scatter band of the SIF-N-curve (Eq. 5) obtained from the notched specimens. This indicates that in the LCF regime a structural hot-spot can be considered as a sharp a crack loaded by a SIF K_{IN}.

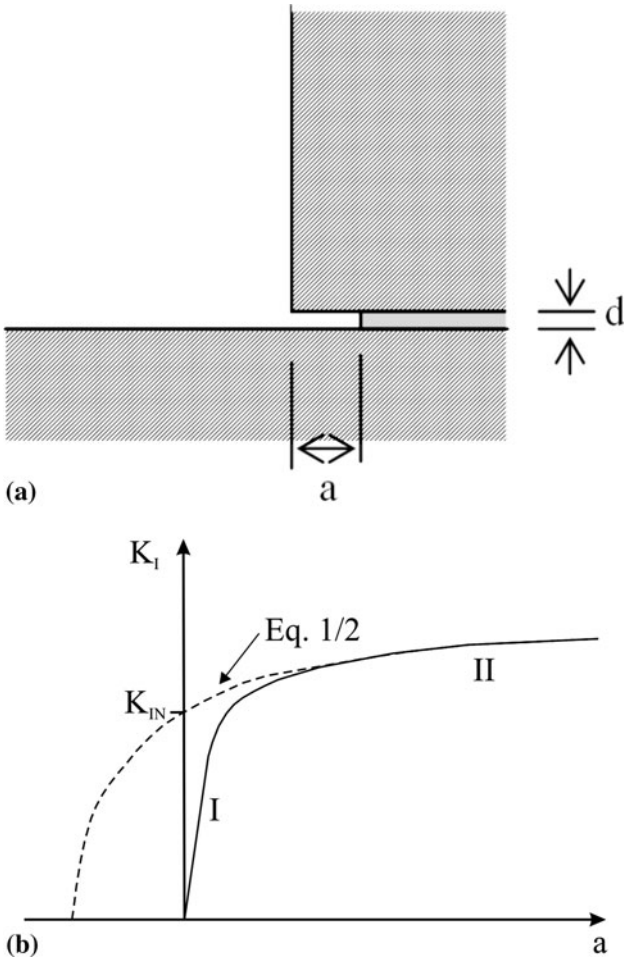

Fig. 9 (a) Geometry and (b) $K_I(a)$ for a short crack in a braze layer emanating from a corner (schematic)

4. Discussion

4.1 Fatigue Assessment Using SIF-N-Curves

The SIF-N-curve allows to estimate the influence of defects or structural hot-spots characterized by a high ratio of the defect length a and the tip radius ρ ($a/\rho \gg 0$) on the integrity of brazed components. As described above, such defects can, e.g., arise from incomplete wetting and gap filling during brazing. In this case, ΔK has to be calculated for an equivalent or conservatively estimated crack of the same geometry and size.

Structural hot-spots can be treated analogously by determining the notch-intensity factor ΔK_{IN}. It is obtained by

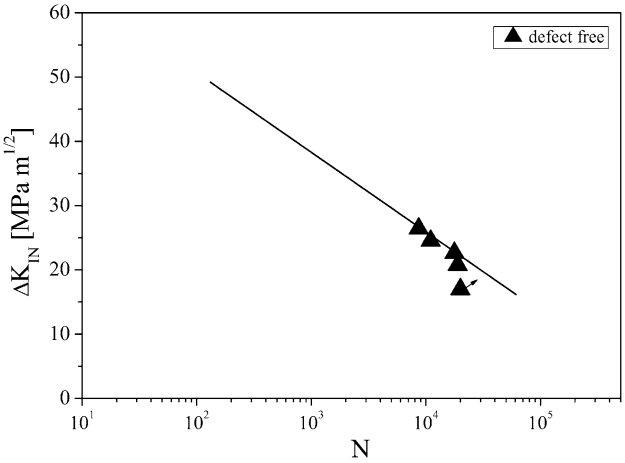

Fig. 10 Fatigue life of defect-free specimens as a function of ΔK_{IN}, in comparison with SIF-N-curve according to Fig. 7

calculating $K(a_n)$ for the initial defect sizes a and extrapolating the resulting curve to $a = 0$.

Strictly speaking, the SIF-N-curves shown in Fig. 7 is only applicable for the defect- and braze-parameters used for the presented experiments ($d = 0.1$ mm, $\rho = 0.15$ mm, and $R = 0.1$). If the deviations of the actual parameters are substantial, corresponding experimental data are required. However, to some degree it is possible to generalize the presented results, at least as approximations.

In homogeneous materials, the notch root radius is crucial for the crack-initiation life, since it affects the local stresses and strains. In the case of a notched brazed specimens, the situation is more complex, since the width of the braze layer and the mismatch of the material parameters represent additional characteristics. The experimental finding that the SIF-N-data of defect-free T-joint specimens fit very well to the data from straight or elliptical notches indicates that the root radius of notches in brazings are of minor importance. Parameters related to the brazing, like the thickness d of the layer, are of more importance.

The effect of the width of the braze layer, d, on the da/dN-curve has been considered theoretically in Ref 27. It was found that the ΔK_{th} is proportional to $d^{1/4}$ and that the da/dN-curve is roughly proportional to $1/d$. This affects the SIF-N-curve in the high-cycle regime and the endurance limit.

It has also been shown that the fracture toughness is associated with a certain critical strain in the layer (Ref 19). In general, the latter is proportional to K_I^2/d, so K_{Ic} is proportional to $d^{1/2}$. It can be expected for physical reasons that K_{fc} and the SIF-N-curve in the LCF-regime are about proportional to $d^{1/2}$ as well. Therefore, the SIF-N-curve shown in Fig. 7 is expected to be conservative if the actual layer thickness d is larger than the one of the specimens used here, which is about 0.1 mm.

The motivation of the present investigation was the safety assessment of brazed components for start/stop-loading cycles that can occur during service of, e.g., compressor or turbine parts, which are relatively few in number and correspond in general to a load ratio $R \approx 0$. For practical reasons, the experimental fatigue tests were performed at $R = 0.1$. The fatigue data in the LCF-regime are expected to be affected by R. For $R < 0.1$, they are conservative, but for $R > 0.1$ they are likely to be non-conservative.

4.2 Estimation of the Entire SIF-N-Curve

The SIF-N-curve given by Eq 5 holds in the range covered by the experimental data, which is about $22 < \Delta K < 40$ MPa $m^{0.5}$. In terms of $\Delta K(a_n)$, the total possible range of finite fatigue life is $\Delta K_{th} < \Delta K(a_n) < K_{cf}(1 - R)$, which means, for the properties of the present brazing as given in Ref 26, about $9 < \Delta K_I < 45$ MPa $m^{0.5}$. Obviously, a large part of the total range of finite fatigue life is covered by LCF. The relatively narrow missing parts can be covered approximately by the following semi-empirical extrapolations.

As mentioned before, the crack initiation life can be estimated by Eq 6 from the total life (Eq 5) and N_{prop}. In mathematical terms, the relation between N_{prop} and $\Delta K(a_n)$ shown in Fig. 8 is found by linear regression to be approximately

$$\log \Delta K_I(a_n) = 1.6721 - \frac{1}{n_{Paris}} \cdot \log N_{prop}. \qquad \text{(Eq 15)}$$

By Eq 1, 5, and 15, one obtains N_{ini} as a function of $\Delta K(a_n)$ for straight defects. The corresponding fraction of fatigue initiation life with respect to the total life, N_{ini}/N_{tot}, is shown in Fig. 11. For $\Delta K > 25$ MPa $m^{0.5}$ nearly the entire life is spent in the initiation phase. For decreasing ΔK (Fig. 11) the fraction of N_{ini} decreases. As ΔK approaches the fatigue crack growth threshold ΔK_{th}, $N_{ini}/N_{prop}$is obviously bound to approach zero. The relatively small gap between the lowest experimental data point, 22.5 MPa $m^{0.5}$, and ΔK_{th} can be bridged with sufficient accuracy by a linear interpolation, as shown by the dashed line in Fig. 11. This interpolation enables the SIF-N-curve to be estimated from (Eq. 15) even in the HCF-regime up to endurance. The resulting curve is shown in Fig. 12. For comparison (Eq 15), which is a lower bound of the total life is also shown. Therefrom one can see that the interpolation affects only the transition from the SIF-N-curve of the LCF-range (Eq 5 to 15), which represents a lower bound in the HCF range. An alternative, conservative way to estimate the total SIF-N-curve (from the low-cycle to the high-cycle regime) is to neglect the transition by just using Eq 5 for $N < N_{is}$ and Eq 15 for $N > N_{is}$, where N_{is} is N at the intersection of these two curves (Fig. 12).

The gap on the lower end of the SIF-N-curve, i.e., between the highest experimentally covered ΔK_I and the critical fatigue

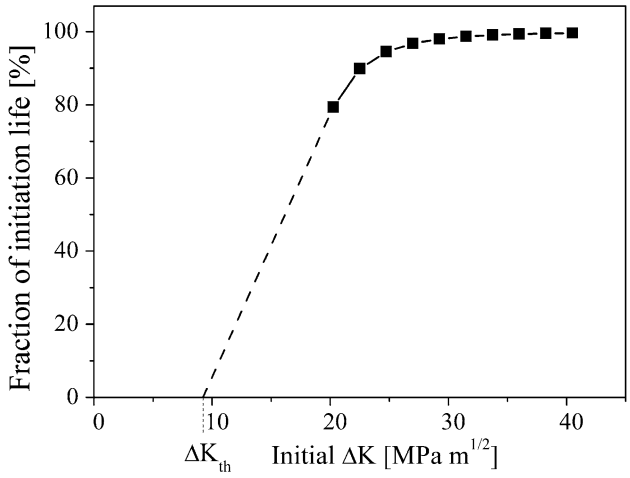

Fig. 11 Portion of Initiation life with respect to total life, N_{ini}/N_{tot}, as a function of the SIF

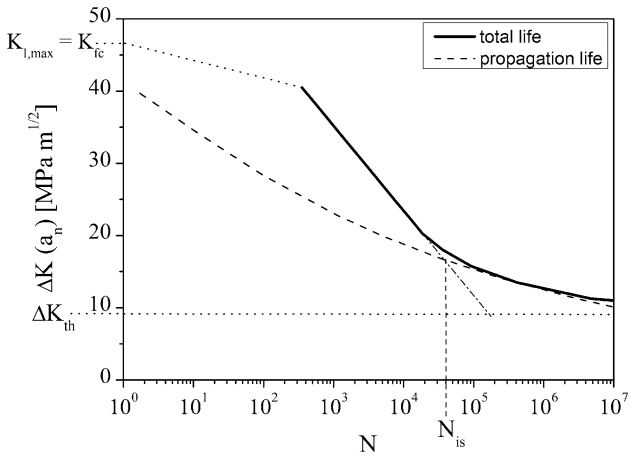

Fig. 12 Total fatigue life estimated from the LCF-tests data and calculated propagation life

load range $K_{cf}(1-R)$, which is the cut-off of the curve at $K_{cf}(1-R)$, can be bridged by another interpolation. For this purpose, using a straight line is expected to be sufficient in general, since this lower range of LCF is usually of minor practical importance. The entire obtained SIF-N-curve is shown in Fig. 12.

The course of ΔK as a function of the total service life N shows that the corresponding coordinate in the SIF-N-diagram has to be located on the left-hand side of the graph in Fig. 12 to guarantee the safe life of the component. Vice versa, for a given nominal stress and a required service life, the SIF-N-curve allows to determine the maximum tolerable defect size.

5. Conclusions

In the scope of the performed experiments, a method was developed to estimate the fatigue lifetime of brazed components under the influence of brazing defects. Based on cyclic loading experiments, the influence of the specimen geometry and of different defects was determined. The resulting S-N-curves show that brazing defects considerably affect the joint strength, but a direct comparison of different defect types based on S-N-curves is not possible. To estimate the influence of different defects, fracture mechanical investigations were performed. The results show that the total life of notched brazings is correlated by $\Delta K(a_n)$. This approach allows structural hot-spots to be treated analogously using the notch SIF K_{IN}. Theoretical investigations show that in the LCF-regime, total life is dominated by initiation process, whereas in the HCF-range, total life is dominated by crack propagation life. This behavior allows the entire SIF-N-curve to be determined and the amount of experimental investigations to be reduced significantly. For different brazing conditions, e.g., for different layer thicknesses, the applicability could already be shown, but further experiments must be performed to investigate the influence of, e.g., different heat treatments.

Acknowledgments

The present work was financially supported by MAN Turbo AG, Zurich, which is gratefully acknowledged. The authors would like to thank Dr. T. A. Baser for her support during the experiments.

References

1. L. Sáncheza, D. Carrillo, E. Rodrígueza, F. Aragóna, J. Sotelob, and F. Torala, Development of High Precision Joints in Particle Accelerator Components Performed by Vacuum Brazing, *J. Mater. Process. Technol.*, 2011, **211**, p 1379–1385
2. R.K. Shiue, S.K. Wu, and S.Y. Chen, Infrared Brazing of TiAl Intermetallic Using BAg-8 Braze Alloy, *Acta Mater.*, 2001, **51**, p 1991–2004
3. T. Ma, M. Zeng, Y. Ji, H. Zhu, and Q. Wang, Investigation of a Novel Bayonet Tube High Temperature Heat Exchanger with Inner and Outer Fins, *Int. J. Hydrogen Energy*, 2011, **36**, p 3757–3768
4. S.L. Feldbauer, Modern Brazing of Stainless Steel, *Am. Weld. Soc. J.*, 2004, **10**, p 30–33
5. J. Novacki and P. Swider, Producibility of Brazed High-Dimension Centrifugal Compressor Impellers, *J. Mater. Process. Technol.*, 2003, **133**, p 174–180
6. M.E. Kassner, T.C. Kennedy, and K.K. Schrems, The Mechanism of Ductile Fracture in Constrained Thin Silver Films, *Acta Mater.*, 1998, **46**, p 6445–6457
7. J. Cugnoni, J. Botsis, and J. Janczak-Rusch, Size and Constraining Effects in Lead-Free Solder Joints, *Adv. Eng. Mater.*, 2006, **8**, p 184–191
8. A.G. Varias, Z. Suo, and C.F. Shih, Ductile Failure of a Constrained Metal Foil, *J. Mech. Phys. Solids*, 1991, **39**, p 963–986
9. M.Y. He, A.G. Evans, and J.W. Hutchinson, Interface Cracking Phenomena in Constrained Metal Layers, *Acta Mater.*, 1996, **44**, p 2963–2971
10. Y. Flom, L. Wang, M.M. Powell, M.A. Soffa, and M.L. Rommel, Evaluating Margins of Safety in Brazed Joints, *Am. Weld. Soc. J.*, 2009, **10**, p 31–37
11. S.H. Choi, B.G. Song, K.J. Kang, and N.A. Fleck, Fracture of a Ductile Layer Constrained by Stiff Substrates, *Fatigue Fract. Eng. Mater. Struct.*, 2001, **23**, p 1–13
12. S. Roy Chowdhury and R. Narasimhan, Finite Element Simulations of Ductile Rupture in a Constrained Metal Foil, *Mater. Sci. Eng. A*, 1995, **191**, p 27–37
13. D.M. Jacobsen and G. Humpston, *Principles of Brazing*, ASM International, Materials Park, OH, 2005
14. Y.J. Kim, M. Koçak, R.A. Ainsworth, and U. Zerbst, SINTAP Defect Assessment Procedure for Strength Mismatched Structures, *Eng. Fract. Mech.*, 2000, **67**, p 529–546
15. British Energy Generation Ltd., Assessment of the Integrity of Structures Containing Defects. R6-Rev. 4, 2002
16. British Standard, Guide on methods for assessing the acceptability of flaws in metallic structures. BS 7910, 1999
17. S. Webster and A. Bannister, Structural Integrity Assessment Procedure for Europe—of the SINTAP Programme Overview, *Eng. Fract. Mech.*, 2000, **67**, p 481–514
18. C. Leinenbach, H. Lehmann, and H.J. Schindler, Mechanical Behaviour and Defect Sensitivity of High Temperature Braze Joints, *MP Mater. Test.*, 2007, **49**, p 2–9 (in German)
19. C. Leinenbach, H.J. Schindler, T.A. Baser, N. Rüttimann, and K. Wegener, Quasistatic Fracture Behaviour and Defect Assessment of Brazed Soft Martensitic Stainless Steel Joints, *Eng. Fail. Anal.*, 2010, **17**, p 672–682
20. H.D. Solomon, A Statistical Analysis of Brazed Joints Fatigue Behaviour, *Weld. Res. Suppl.*, 2001, **6**, p 148–156
21. C. Leinenbach, N. Gelder, V. Bissig, F. Gattiker, and U.E. Klotz, Shielding Gas Brazing of Martensitic Stainless Steels with Copper Free Silver Based Filler Metals, *Sci. Technol. Weld. Join.*, 2007, **12**, p 708–717
22. B. Chen and D.A. Dillard, Numerical Analysis of Directionally Unstable Crack Propagation in Adhesively Bonded Joints, *Int. J. Solid. Struct.*, 2001, **38**, p 6907–6924
23. S. Azari, M. Papini, J.A. Schroeder, and J.K. Spelt, The Effect of Mode Ratio and Bond Interface on the Fatigue Behavior of a Highly-Toughened Epoxy, *Eng. Fract. Mech.*, 2010, **77**, p 395–414
24. R.O. Ritchie, R.M. Cannon, B.J. Dalgleish, R.H. Dauskardt, and J.M. McNaney, Mechanics and Mechanisms of Crack Growth at or Near Ceramic-Metallic Interfaces, *Mater. Sci. Eng.*, 1993, **166**, p 221–235
25. T.A. Baser, C. Leinenbach, and H.J. Schindler, Cyclic Fracture Behaviour of Brazed Martensitic Stainless Steel Joints. *Proceedings of the ICF 12*, 2009
26. T.A. Baser, C. Leinenbach, and H.J. Schindler, Fracture Behaviour of Brazed Soft Martensitic Stainless Steel Joints Under Cyclic Loading, *Mater. Sci. Forum*, 2010, **636–637**, p 1490–1495
27. H.J. Schindler, and C. Leinenbach, Mechanics of Fatigue Crack Growth in a Bonding Interface. *Eng. Fract. Mech.* (in press)
28. S. Li, L. Sun, W. Jia, and Z. Wang, The Paris Law in Metals and Ceramics, *J. Mater. Sci. Lett.*, 1995, **14**, p 1493–1495
29. H.J. Schindler, and C. Leinenbach: Fatigue Assessment of Brazed T-Joints Based on Damage Tolerance Including Residual Stress Effects. J. ASTM Int., 2010, **7**, 102515
30. H.J. Schindler, Endurance Assessment for Notched Structural Parts with Imperfections. *DVM Rep.*, 2002, **234**, 67–76